

Lithium Ion Transport Mechanism in Ternary Polymer Electrolyte-Ionic Liquid Mixtures – A Molecular Dynamics Simulation Study

Diddo Diddens^{1,2,*} and Andreas Heuer^{1,2}

¹*Institut für physikalische Chemie, Westfälische Wilhelms-Universität
Münster, Corrensstrasse 28/30, 48149 Münster, Germany*

²*NRW Graduate School of Chemistry, Corrensstrasse 36, 48149 Münster, Germany*

(Dated: November 1, 2018)

The lithium transport mechanism in ternary polymer electrolytes, consisting of PEO₂₀LiTFSI and various fractions of the ionic liquid PYR₁₃TFSI, is investigated by means of MD simulations. This is motivated by recent experimental findings¹, which demonstrated that these materials display an enhanced lithium mobility relative to their binary counterpart PEO₂₀LiTFSI. In order to grasp the underlying microscopic scenario giving rise to these observations, we employ an analytical, Rouse-based cation transport model², which has originally been devised for conventional polymer electrolytes. This model describes the cation transport via three different mechanisms, each characterized by an individual time scale. It turns out that also in the ternary electrolytes essentially all lithium ions are coordinated by PEO chains, thus ruling out a transport mechanism enhanced by the presence of ionic-liquid molecules. Rather, the plasticizing effect of the ionic liquid contributes to the increased lithium mobility by enhancing the dynamics of the PEO chains and consequently also the motion of the attached ions. Additional focus is laid on the prediction of lithium diffusion coefficients from the simulation data for various chain lengths and the comparison with experimental data, thus demonstrating the broad applicability of our approach.

PACS numbers:

I. MOTIVATION

Solid polymer electrolytes (SPEs) are promising candidates for lithium ion batteries, as they are ideal to create small and light-weighted but powerful energy storages^{3,4}. The classical SPEs consist of an amorphous polymer matrix, e. g. poly(ethylene oxide) (PEO), and a lithium salt dissolved in it^{5,6}. By using lithium salts with large anions such as lithium-bis(trifluoromethane)sulfonimide (LiTFSI), the crystallization can be suppressed as the negative charge is delocalized over the whole anion. However, at ambient temperatures, the conductivity of most SPEs is still too low for an efficient technological use. Among several other remedies^{7–10}, the incorporation of a room temperature ionic liquid (IL) seems to be a very promising approach^{1,11}, as the resulting ternary electrolytes show both an increased conductivity and inherent stability. Moreover, ILs are non-volatile, non-flammable¹² and exhibit a wide electrochemical stability window¹³.

However, it is not yet fully understood in how far the lithium transport mechanism in these materials changes relative to the conventional polymer electrolytes. For instance, it was speculated¹¹ that the lithium ions become progressively coordinated by the anions from the IL and are thus decoupled from the rather slow PEO chains. Alternatively, one might also expect that the IL enhances the PEO dynamics and serves as a plasticizer in this way, which is a common observation when adding low-molecular solvents to PEO-salt systems^{8–10}. In this work, we utilize molecular dynamics (MD) simulations to unravel the impact of the addition of IL. In order to quantify the lithium motion, we employ an analytical cation

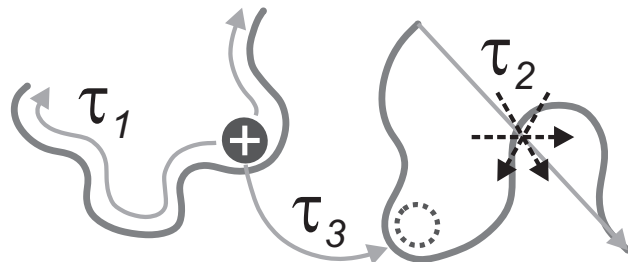


Figure 1: Scheme illustrating the three cation transport mechanisms in PEO-salt electrolytes.

transport model^{2,14}, which has originally been devised for binary polymer electrolytes.

Our description is based on both the Rouse model¹⁵ as well as the Dynamic Bond Percolation (DBP) model¹⁶, and distinguishes three different microscopic lithium ion transport mechanisms (Figure 1): 1. The ions diffuse along the PEO backbone to which they are attached. This motion can be characterized by the time scale τ_1 the ions need to explore the entire PEO chain. 2. For ambient temperatures, the PEO chains are naturally also subject to thermal motion, carrying the attached ions in this way. In case of Rousean motion, the polymer dynamics and thus motion of the attached ions can be quantified by an effective Rouse time τ_2 . 3. Finally, an ion bound to a specific PEO chain can be transferred to another chain. The mean residence time at a given chain is denoted as τ_3 in the following. As demonstrated earlier², the last mechanism can also be viewed as a renewal process within the framework of the DBP model.

Of course, for the ternary electrolytes, it is a priori

unclear if this scenario changes only quantitatively – reflected by different values for τ_1 , τ_2 and τ_3 – or if the lithium ion transport mechanism also changes on a qualitative level. In particular, we focus on two ternary polymer electrolytes with the same IL as in ref. 11, i. e. *N*-methyl-*N*-propylpyrrolidinium TFSI (PYR₁₃TFSI), with a stoichiometry of PEO₂₀LiTFSI · 0.66 PYR₁₃TFSI and PEO₂₀LiTFSI · 3.24 PYR₁₃TFSI, respectively. The binary polymer electrolyte, PEO₂₀LiTFSI, serves as a reference. For convenience, PEO will be abbreviated as ‘P’ and LiTFSI as ‘S’ in the following, leading to the shorthand notation P₂₀S · x IL with $x = 0$, $x = 0.66$ and $x = 3.24$.

II. SIMULATION DETAILS

The simulations were performed with the AMBER 10 package¹⁷. Here, the sander module was modified, allowing us to use a many-body polarizable force field specifically designed for PEO/LiTFSI^{18,19} and PYR₁₃TFSI²⁰. The simulation box contained 10 PEO chains with $N = 54$ monomers each as well as 27 LiTFSI ion pairs, yielding a concentration of ether oxygens (EOs) to lithium ions of 20 : 1. Additionally, the two ternary systems contained 18 or 87 PYR₁₃TFSI molecules, corresponding to $x = 0.66$ and $x = 3.24$. The simulation cells have been created randomly in the gas phase to yield homogeneous systems. After equilibration runs of 70 – 80 ns in the NpT ensemble, production runs with a length of 200 ns have been performed in the NVT ensemble, collecting data every picosecond. An elementary integration step of 1 fs was used, while the systems were coupled to a Berendsen thermostat²¹ with a reference temperature of 423 K. All bonds involving hydrogen were constrained by the SHAKE algorithm²². The inducible point dipoles were integrated by a Car-Parrinello-like scheme²³. By comparing various radial distribution functions and mean square displacements (MSDs) for the first and the second half of the runs, we confirmed that the systems are in equilibrium. Moreover, the former showed no long-range ordering, demonstrating that the systems are perfectly mixed.

III. STRUCTURAL PROPERTIES

A. Lithium Ion Coordination

We find for all electrolytes that virtually all lithium ions are coordinated to one or two PEO chains, thereby giving a first hint that also for the ternary systems the cation transport entirely takes place at the PEO chains. The percentages of lithium ions coordinating to one or two PEO chains is given in Table I. With increasing IL concentration, the probability that a lithium ion coordinates to two PEO chains decreases, thus indicating a dilution effect which reduces the probability for an ion to

system	1 PEO [%]	2 PEO [%]
P ₂₀ S	47.2	52.7
P ₂₀ S · 0.66 IL	53.0	47.0
P ₂₀ S · 3.24 IL	75.8	24.0

Table I: Ratio of lithium ions coordinating to one or two PEO chains.

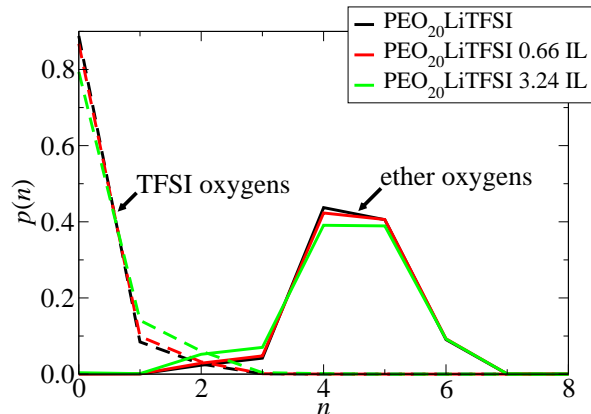


Figure 2: Probability $p(n)$ to find a certain coordination number n of EOs (irrespective if the ion is tied to one or two PEO chains) or TFSI oxygens.

encounter a second PEO molecule. This is also supported by the observation that the amount of Li⁺ coordinating two PEO chains decreases linearly with x .

The predominant lithium coordination consists of 4–5 EOs (see Figure 2, which shows the probability distribution functions $p(n)$ to find a lithium ion with n EOs or TFSI oxygens in its first coordination shell), which is in good agreement with experimental data²⁴ and quantum chemistry calculations^{25,26}. In those complexes where the 4–5 EOs originate from a single PEO molecule, the polymer chain wraps helically around the cation. For complexes involving two PEO chains, typically 2–3 EOs from each chain coordinate to the ion. Additional coordinations by TFSI oxygens are rather rare (about 12–20 %, see Figure 2), and in most cases the anion coordinates only briefly to the lithium ion. Again, the amount of Li⁺ coordinating to TFSI increases linearly with x , thus indicating that this effect is purely statistical.

B. Statical Polymer Properties

For the conformational properties of the PEO molecules, we naturally observe a contraction of the chains due to the crown-ether-like coordination sphere of the lithium ions²⁷. This manifests itself by a decrease of the mean squared end-to-end vector $\langle \mathbf{R}_e^2 \rangle$ for the electrolytes ($\langle \mathbf{R}_e^2 \rangle = 1662 \text{ \AA}^2$, 1570 \AA^2 and 1571 \AA^2

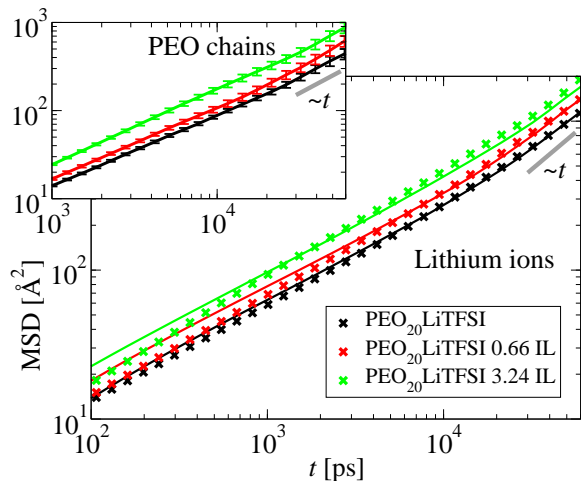


Figure 3: MSD of the lithium ions (main panel) and the center of mass of the PEO chains (inset). The solid lines in the main panel correspond to the model predictions.

for $x = 0, 0.66$ and 3.24 , respectively) as compared to the pure PEO melt ($\langle \mathbf{R}_e^2 \rangle = 1979 \text{ \AA}^2$). In case of the ternary electrolytes, one might expect that the PEO chains are swollen on a global scale, since the addition of IL would induce a crossover from a polymer melt to a semidilute solution. However, from both $\langle \mathbf{R}_e^2 \rangle$ and the scaling of the Rouse-mode amplitudes^{15,28} (not shown), we observe no such feature.

IV. DYNAMICS OF THE LITHIUM IONS

Although from a structural point of view no significant differences emerge, we observe a clear increase of the lithium MSD, especially for the subdiffusive regime at $t = 1 - 10 \text{ ns}$ (crosses in Figure 3), whereas the onset to diffusion occurs on comparable time scales, i. e. $t = 20 - 50 \text{ ns}$. A similar increase can be found for the MSD of the entire PEO chains (inset of Figure 3). In the following, we will go more into detail and investigate the relative importance of the individual transport mechanisms.

A. Interchain Transfer

In order to calculate the renewal times, the number of transfer processes N_{tr} was counted from the simulations, and the τ_3 -values were determined according to $\tau_3 = t_{\text{max}} N_{\text{Li}^+} / N_{\text{tr}}$, where $t_{\text{max}} = 200 \text{ ns}$ is the simulation length and $N_{\text{Li}^+} = 27$ is the number of lithium ions in the simulation box. Of course, it is questionable if brief transfers followed by successive backjumps to the previous polymer chain serve as a renewal process in the strict sense, since the lithium dynamics will not become uncorrelated to its past after such an event. A more

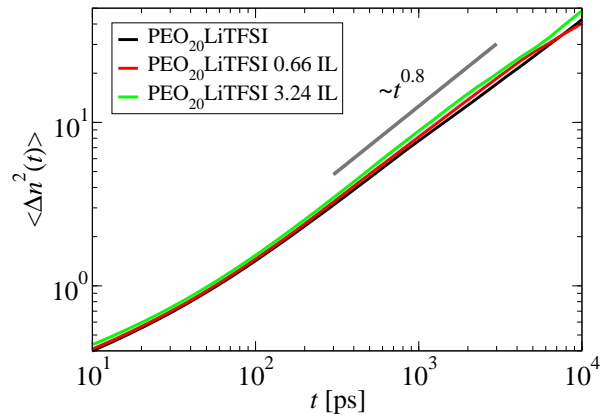


Figure 4: MSD of the average EO index $\langle \Delta n^2(t) \rangle$.

detailed analysis (not shown) revealed that these non-Markovian, short-time backjumps occurred up to 100 ps , which we used subsequently as a criterion to define real renewal events. In cases where the transfer was mediated by TFSI anions only (probability p_{IL} in Table II), we found that the displacement the ion covers in the IL-rich region was sufficiently small, so that the contribution of these transfers to the lithium MSD is negligible.

We observe that τ_3 (Table II) increases with increasing IL concentration. Since the PEO molecules become more and more diluted, this can mainly be explained as a concentration effect. Obviously, the critical step for a transfer process is the encounter of a another PEO segment.

B. Motion Along the PEO Backbone

In order to quantify the diffusion along the PEO backbone, we successively numbered all monomers at a given PEO chain, allowing us to express the lithium position by the average EO index n , and to calculate an effective MSD $\langle \Delta n^2(t) \rangle$ along this coordinate (Figure 4). We find that this type of motion is slightly subdiffusive (i. e. $\langle \Delta n^2(t) \rangle \propto t^{0.8}$) for all electrolytes within the statistical error. No significant dependence on the IL concentration can be observed. This indicates that the surrounding molecules (PEO chains or IL) have no influence on this mechanism. Moreover, also the magnitude of $\langle \Delta n^2(t) \rangle$ is essentially the same for lithium ions bound to one or to two PEO chains (not shown).

Note that the statistics of the $\langle \Delta n^2(t) \rangle$ -curves in Figure 4 are insufficient for $t > 10 \text{ ns}$, wherefore the plot is only shown up to 10 ns . This is due to the fact that the lithium ions are transferred to other PEO chains, and the motion cannot be tracked any further in a reliable manner, even though in some cases the ion jumps back to the first chain after some picoseconds. For sufficiently long chains as well as a significant amount of PEO-Li⁺ complexes that exist throughout the entire observation time, $\langle \Delta n^2(t) \rangle$ will show diffusive behavior on longer time

x_{IL}	τ_1 [ns]	$\langle \mathbf{R}_c^2 \rangle$ [\AA^2]	τ_R [ns]	τ_2 [ns]	τ_3 [ns]	p_{IL} [%]	$D_{\text{Li}}^{\text{sim}}$ [$\text{\AA}^2 \text{ns}^{-1}$]	D_{Li}^{∞} [$\text{\AA}^2 \text{ns}^{-1}$]	$D_{\text{Li}}^{\text{exp}}$ [$\text{\AA}^2 \text{ns}^{-1}$]
0.0	147	1662	45	167	17	2.5	2.945	1.947	0.052 ($x = 0.0$)
0.66	140	1570	37	89	18	1.0	3.542	2.309	0.118 ($x = 1.0$)
3.24	127	1571	24	68	24	8.5	4.257	2.392	0.126 ($x = 4.0$)

Table II: Parameters characterizing the three transport mechanisms (see text for further explanation).

scales. Naturally, in the limit $t \rightarrow \infty$, one would expect a crossover to a plateau for finite chain lengths. From $\langle \Delta n^2(t) \rangle$, neither of these two effects can be found, indicating that most life times of the PEO–Li⁺ complexes are too short. Rather, the lithium ions only move on average 7–8 monomers during 10 ns. Keeping in mind that the lithium ions are typically bound to 4–5 monomers, these findings imply that the ions have barely left their own coordination sphere during the accessible time scale. Therefore, finite size effects of the PEO chains are irrelevant in the present case.

In principle, the motion along the PEO chain can be quantified by an effective diffusion coefficient D_1 , which can be calculated from the $\langle \Delta n^2(t) \rangle$ -curves according to

$$D_1 = \frac{\langle \Delta n^2(t) \rangle}{2t}. \quad (1)$$

However, due to the subdiffusivity of $\langle \Delta n^2(t) \rangle$, the D_1 values depend on the specific time for which they are estimated. Thus, in order to estimate the net effect of this mechanism, one would ideally compute D_1 at $t = \tau_3$, for which the statistics are unfortunately too bad due to reasons mentioned above. As an approximation, we extrapolated the $\langle \Delta n^2(t) \rangle$ -curves in Figure 4 under the assumption that the scaling $\langle \Delta n^2(t) \rangle \propto t^{0.8}$ persists until $t = \tau_3$. In order to estimate the net effect of this mechanism (i. e. the number of traversed monomers before the ion is transferred to another chain), we define τ_1 via²

$$\tau_1 = \frac{(N-1)^2}{\pi^2} \frac{2\tau_3}{\langle \Delta n^2(\tau_3) \rangle}, \quad (2)$$

which due to the subdiffusivity of $\langle \Delta n^2(t) \rangle$ slightly depends on τ_3 . One observes that τ_1 decreases slightly with increasing IL concentration (Table II), reflecting the weak dependence of τ_1 on τ_3 .

C. Polymer Motion

Figure 5 shows the MSD of the EOs relative to the center of mass of the PEO chain. This quantity has been computed for all EOs (i. e. irrespective of the presence of an ion), for EOs bound to a lithium ion as well as for the respective attached ions. The criterion to consider a cation or EO as bound was that the average EO index of the ion did not change more than one, i. e. $|\Delta n(t)| \leq 1$ for all time frames during t . For the bound EOs, no further distinction between additional coordinations of the lithium ion to another PEO chain or a TFSI

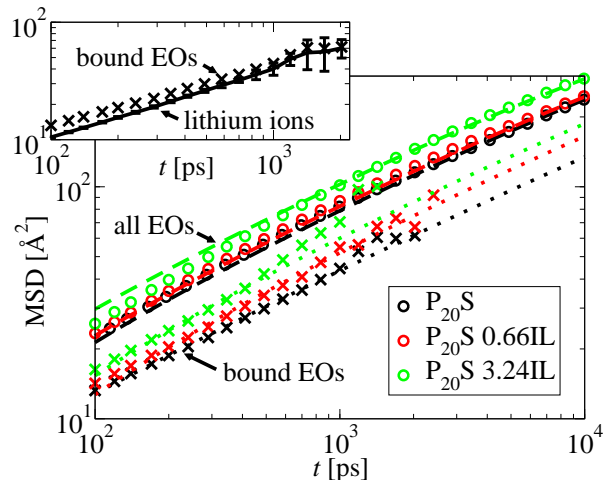


Figure 5: MSDs of the average EOs (circles), the bound EOs (crosses) and the lithium ions bound to these EOs (inset, solid lines). The dashed and dotted lines show the respective Rouse fits.

molecule was made. Thus, these effects are already implicitly contained in the curves in Figure 5. Of course, it is questionable if cations bound to two PEO chains show the same dynamics as ions bound to one chain only, since the former could be regarded as transient crosslinks, which would significantly impede the polymer motion. A more detailed analysis indeed revealed that there is a conceptual difference between these two coordinations, however, this effect can easily be taken into account (see Appendix A) and does not affect the general formalism of our analysis.

The average EOs (circles) show typical Rouse-like motion with the characteristic relaxation time τ_R . The dynamics of the bound EOs (crosses) is qualitatively the same but protracted. Therefore, it is possible to characterize the dynamics of the bound EOs by a larger, effective Rouse time τ_2 . The lithium ions attached to these EOs (shown in the inset of Figure 5 for P₂₀S, the curves for the other electrolytes look similar) closely follow the bound EOs, which gives clear evidence for their cooperative motion. On short time scales, the MSD of the EOs is larger than the lithium MSD due to the additional internal degrees of freedom of the PEO backbone, but the MSD of the bound cations catches up at $t \approx 1$ ns. Thus, τ_2 characterizes both the dynamics of the bound PEO segments as well as of the attached lithium ions.

Figure 5 also shows the Rouse fits, i. e. $g_R(t) =$

$2\langle \mathbf{R}_e^2 \rangle \pi^{-2} \sum_{p=1}^{N-1} [1 - \exp(-tp^2/\tau_R)] p^{-2}$, for the average (dashed lines) and for the bound EOs (dotted lines). Of course, the precise value of τ_R and τ_2 also depends on the value of $\langle \mathbf{R}_e^2 \rangle$. In order to obtain a fit consistent with the plateau value at large t (not shown in Figure 5 for clarity), the MSDs of the average EOs were fitted using two parameters, i.e. τ_R and $\langle \mathbf{R}_e^2 \rangle$. Subsequently, the MSDs of the bound EOs were fitted using this value in combination with a single fit parameter τ_2 only (Table II, deviations from our previous study¹⁴ on P₂₀S arise from the shorter simulation length of about 27 ns and the modified fitting procedure).

Whereas the $\langle \mathbf{R}_e^2 \rangle$ -values are approximately constant, both τ_R and τ_2 decrease significantly, clearly indicating that the dynamics of the PEO segments becomes faster with increasing IL concentration. Therefore, the IL can be regarded as plasticizer. For the average segments, the dynamics for P₂₀S · 3.24 IL is nearly the same as for pure PEO ($\tau_R = 22$ ns), showing that the plasticizing approximately cancels with the slowing-down caused by the coordinating lithium ions as found for P₂₀S. The presence of the IL also enhances the motion of the bound segments, and, as a result, the dynamics of the respective attached lithium ions, leading to an increase of the overall lithium MSD. Here, experimental studies reported similar findings for other plasticizers like ethylene/propylene carbonate^{9,10} or short PEO chains embedded in a high-molecular weight matrix^{8,10}.

For finite N , the plasticizing effect is even twofold. Apart from the internal, segmental PEO dynamics (Figure 5), the center-of-mass motion is also accelerated by the addition of IL (inset of Figure 3). The relative importance of these two types of plasticizing will be discussed below.

V. APPLICATION OF THE TRANSPORT MODEL

As a consistency check of our description, we employ the transport model to reproduce the lithium MSD in Figure 3. During the residence time \tilde{t} at a given PEO chain, the MSD g_{12} of the lithium ion is given by a Rouse-like expression²

$$g_{12}(\tilde{t}) = \frac{2\langle \mathbf{R}_e^2 \rangle}{\pi^2} \sum_{p=1}^{N-1} \frac{[1 - \exp(-\frac{\tilde{t}p^2}{\tau_{12}})]}{p^2}, \quad (3)$$

where $\tau_{12}^{-1} = \tau_1^{-1} + \tau_2^{-1}$ is a combined relaxation rate due to both intramolecular mechanisms. After a renewal process (i.e. an interchain transfer), the ion dynamics becomes uncorrelated to its past^{2,16}, and the motion at the new chain is again characterized by Eq. 3. Thus, it is possible to interpret the overall lithium dynamics as a random walk, in which the elementary step length is given by Eq. 3, and the direction of motion for the successive step changes randomly after each renewal event.

We assumed that the number of ion transfer processes during time interval t is given by a Poisson distribution with mean t/τ_3 , leading to exponentially distributed \tilde{t} . For a given t , the lithium MSD due to the three transport mechanisms was then obtained from the numerical average over a large number of Poisson processes. The third ingredient required for the total lithium MSD is the center-of-mass motion of the PEO chains, which was directly extracted from the simulations (inset of Figure 3) and added to the model curve. The resulting predictions are shown as solid lines in the main panel of Figure 3, the respective diffusion coefficients $D_{\text{Li}}^{\text{sim}}$ calculated from the model curves are given in Table II.

For P₂₀S, one observes a nearly perfect agreement throughout the entire observation time. This demonstrates that our transport model indeed captures the underlying, much more complex microscopic scenario. In case of P₂₀S · 0.66 IL and P₂₀S · 3.24 IL, the model curves agree with the empirical lithium MSD for time scales larger than about 1 – 2 ns. Slight deviations can be attributed to the large uncertainties of the MSD of the PEO chains. However, the model prediction systematically overestimates the MSDs of P₂₀S · 0.66 IL and P₂₀S · 3.24 IL for short time scales. Here, a more detailed analysis (to be published under separate cover) revealed that these deviations are caused by hydrodynamic interactions arising from the presence of the IL. On larger length and time scales, these hydrodynamic interactions are screened, which has also been reported for other semidilute polymer solutions²⁹. Thus, both the Rouse-like behavior and the diffusive regime are correctly reproduced, which clearly demonstrates the applicability of our model to the experimentally relevant long-time limit.

Finally, we use the same procedure as above to compute D_{Li}^{∞} for $N \rightarrow \infty$ via the scaling laws² $\langle \mathbf{R}_e^2 \rangle \propto N$, $\tau_1 \propto N^2$, $\tau_2 \propto N^2$ and $\tau_3 \propto N^0$. Of course, for the scaling of τ_2 , entanglement effects may become relevant, which would slow down the segmental dynamics. However, if $\tau_3 < \tau_e$ (i.e. the entanglement time), meaning that the lithium ion leaves the PEO chain before the latter begins to reptate, the overall dynamics is still Rousean²⁸, and our model can still be used to calculate D_{Li} . For PEO, experiments³⁰ revealed that the entanglement regime sets in from about $N \approx 75$. Based on these observations, one can estimate τ_e according to $\tau_e = \tau_R(N = 75) = \tau_R(75/54)^2$. For P₂₀S, this leads to $\tau_e \approx 87$ ns, which is substantially larger than τ_3 . Also in case of the highly plasticized P₂₀S · 3.24 IL one finds $\tau_e \approx 46$ ns $>$ τ_3 . Therefore, the lithium ion leaves the PEO chain before the tube constraints become noticeable, and our formalism can also be applied for $N \rightarrow \infty$.

Table II shows D_{Li}^{∞} calculated from the model together with the PFG-NMR data¹ at $T = 323$ K. For the experimental measurements, both the IL fraction x and the IL cation, i.e. PYR₁₄, are slightly different than in our simulations, however, one would expect no significant effect on the transport mechanism. In both cases, we observe

a clear increase of D_{Li} , which can be attributed to the plasticizing effect of the IL.

However, when discussing these values, one has to keep in mind that not only the segmental motion, but also τ_3 and D_{PEO} affect the precise value of D_{Li} , in which each contribution has its own N -dependence. For example, in case of $N \rightarrow \infty$, the mean intramolecular MSD $\langle g_{12} \rangle$ (averaged over all \tilde{t} , Eq. 3), increases by about 28 % for $\text{P}_{20}\text{S} \cdot 0.66$ IL and 73 % for $\text{P}_{20}\text{S} \cdot 3.24$ IL, mainly as a result of the increased segmental mobility. On the other hand, the renewal rate decreases by about 7 % and 29 %, although the plasticizing effect dominates, and the overall D_{Li}^∞ -values increase by about 19 % and 23 %. For $N = 54$, the situation is slightly different. Here, the segmental plasticizing, measured by $\langle g_{12} \rangle$, leads only to an increase of 22 % for $x = 0.66$ and 54 % for $x = 3.24$. Finally, for $N \rightarrow 1$, the differences in $\langle g_{12} \rangle$ would even disappear². However, this trend is compensated by the plasticizing of the center-of-mass motion of PEO. For $N = 54$, D_{PEO} is raised by 30 % for $x = 0.66$ and by 92 % for $x = 3.24$, which results in an overall increase of D_{Li} of 20 % for $\text{P}_{20}\text{S} \cdot 0.66$ IL and 45 % for $\text{P}_{20}\text{S} \cdot 3.24$ IL.

So far, we focused on the high-temperature limit which we can address in our simulations. Interestingly, the relative increase of $D_{\text{Li}}^{\text{exp}}$ upon the addition of IL becomes much more pronounced in the low-temperature regime¹ (see also Table II). Although simulations at low temperatures would be too costly, one might expect that the plasticizing effect at least partly accounts for the larger relative increase of D_{Li} in this regime. Here, DSC measurements¹ revealed that the glass-transition temperature decreases up to 35 K upon IL addition, which gives a first hint that also at low temperatures the enhanced polymer dynamics contributes to the faster lithium motion. In such a scenario, the plasticizing of the polymer matrix via electrochemically stable additives would be an important milestone for the use of SPE-based batteries in electronic devices, as their current limitation particularly holds for low (i. e. ambient) temperatures. In fact, PEO/LiTFSI/IL mixtures have recently been successfully applied in prototype batteries³¹.

VI. CONCLUSION

In this study, we have examined the microscopic lithium ion transport mechanism in ternary polymer electrolytes consisting of $\text{PEO}_{20}\text{LiTFSI}$ and $\text{PYR}_{13}\text{TFSI}$. In particular, we addressed the question in how far the microscopic scenario of the ion transport changes upon the addition of IL, and how the experimentally observed increase in the lithium ion diffusion coefficient¹ can be understood in terms of the individual transport mechanisms. To this purpose, an analytical cation transport model² was successfully applied. It turned out that virtually all lithium ions were coordinated to the PEO chains, thus ruling out a transport mechanism in which the lithium transportation is decoupled from the polymer

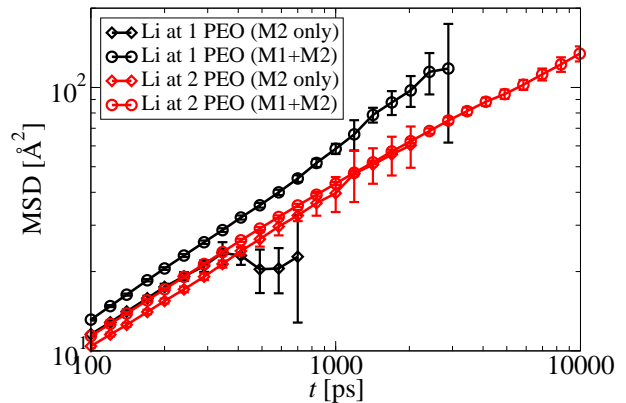


Figure 6: MSDs of the lithium ions bound to one or two PEO chains in $\text{PEO}_{20}\text{LiTFSI}$. A second distinction was made between cations that diffused along the PEO chain (M1 and M2) and ions that remained bound to the same EOs (M2 only). All curves have been computed in the center-of-mass frame. For the other electrolytes, the scenario is qualitatively the same.

chains. Rather, the main reason for the increase of the lithium diffusion coefficient, at least for the considered temperature, is the plasticizing effect of the IL, which enhances the segmental motion of the PEO chains and thus also the dynamics of the attached ions. A minor counter-acting effect was the successive dilution of the electrolyte due to the IL, which slightly decreases the rate of inter-chain transfers. In the sum however, the plasticizing is dominant, and the overall lithium diffusivity increases. For the design of novel battery materials, our findings therefore imply that a polymer electrolyte which is both highly plasticized and exhibits a high transfer rate, e. g. facilitated by a more coordinating IL, would yield optimal results.

Acknowledgments

The authors would like to thank Oleg Borodin, Nicolaas A. Stolwijk, Stefano Passerini and Mario Joost for helpful discussions and for providing the experimental data. Financial support from the NRW Graduate School of Chemistry is also greatly appreciated.

Appendix A: Influence of the Li^+ Coordination on the Segmental Motion

In order to elucidate in how far the lithium ions coordinated to two PEO chains act as temporary crosslinks, Figure 6 shows the MSD of lithium ions bound to one and to two PEO chains for P_{20}S . A second distinction was made if the ions diffused along the PEO chain (i. e. the ion was transported by both intrachain diffusion (M1) and polymer dynamics (M2)) or remained bound to the same EOs (polymer dynamics only, here, the same cri-

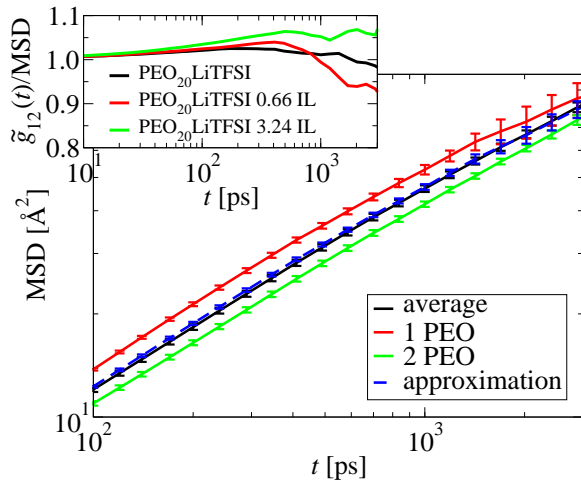


Figure 7: MSD of lithium ions bound to one or two PEO chains as well as the MSD of cations which are bound to the same PEO molecule during t (irrespective of further coordinations) for P₂₀S. The MSDs of ions bound to one and to two chains have been used to compute an approximate average $\tilde{g}_{12}(t)$ according to Eq. A1. Inset: ratio of $\tilde{g}_{12}(t)$ relative to the real average MSD as extracted from the simulations.

terion as for Figure 5 of the main part of our analysis, $|\Delta n(t)| \leq 1$, has been applied). In case of cations bound to one PEO chain only, ions undergoing both types of intramolecular transport are clearly faster than those remaining close to the initial position on the PEO chain (Figure 6). For lithium ions connected to two PEO chains, no significant difference between these two categories can be observed in the MSD (Figure 6). This implies that the cations bound to two PEO chains experience no effective transport due to the diffusion along the chain. Rather, the PEO chain moves reptation-like along its own contour past the cation, which results in a non-zero $\langle \Delta n^2(t) \rangle$, but does not contribute to the overall

lithium transport. For all other investigated electrolytes, the observations from Figure 6 are qualitatively the same.

With respect to the transport model, in particular Eq. 3 in the main body, this effect can be easily captured. Here, the only additionally required parameter is the ratio of lithium ions coordinated to one or two PEO chains (Table I):

$$\tilde{g}_{12}(t) = r_{1\text{PEO}} g_{12}(t) + (1 - r_{1\text{PEO}}) g_2(t) \quad (\text{A1})$$

For the fraction $r_{1\text{PEO}}$ of cations bound to one PEO chain, Eq. 3 remains valid, whereas for ions bound to two chains with $\tau_{1,2\text{PEO}} \rightarrow \infty$ only τ_2 is important. Within this approximation, the average dynamics of the lithium ions (i. e. averaged over ions bound to one or two PEO chains while simultaneously allowing the intermediate exchange between these two coordination states) is estimated from the structural property $r_{1\text{PEO}}$ only.

Figure 7 shows that this rather simplistic picture is indeed valid to a good approximation. Here, Figure 7 displays the MSD of ions bound to one or two PEO molecules in P₂₀S as extracted from the simulations. These curves have in turn been used to calculate an approximate average MSD according to Eq. A1, which is also shown in Figure 7. In fact, the agreement of $\tilde{g}_{12}(t)$ with the average MSD (i. e. a lithium ion that remained on the same chain irrespective of other coordinations) is nearly quantitative. Deviations for larger time scales are due to bad statistics. In the same spirit, the inset of Figure 7 shows the ratio between the approximate $\tilde{g}_{12}(t)$ and the average MSD directly calculated from the simulations for all systems. As for P₂₀S, this ratio is close to unity for all other electrolytes. These observations highlight that, since the crosslinks are temporary and an exchange between both coordination types takes place, the long-time behavior of the intramolecular dynamics may be estimated by the average in Eq. A1, as nicely demonstrated in Figure 7.

* Electronic address: d.diddens@uni-muenster.de

¹ M. Joost, M. Kunze, S. Jeong, M. Schönhoff, M. Winter, and S. Passerini, *Electrochim. Acta* **86**(0), 330 (2012).

² A. Maitra and A. Heuer, *Phys. Rev. Lett.* **98**(22), 227802 (2007).

³ F. M. Gray, *Solid Polymer Electrolytes* (Wiley-VCH, New York, 1991).

⁴ P. G. Bruce and C. A. Vincent, *J. Chem. Soc. Faraday Trans.* **89**(17), 3187 (1993).

⁵ D. E. Fenton, J. M. Parker, and P. V. Wright, *Polymer* **14**(11), 589 (1973).

⁶ M. B. Armand, *Ann. Rev. Mater. Sci.* **16**, 245 (1986).

⁷ W. Gang, J. Roos, D. Brinkmann, F. Capuano, F. Croce, and B. Scrosati, *Solid State Ionics* **53**(Part 2), 1102 (1992).

⁸ M. C. Borghini, M. Mastragostino, and A. Zanelli, *Electrochim. Acta* **41**(15), 2369 (1996).

⁹ L. R. A. K. Bandara, M. A. K. L. Dissanayake, and B. E. Mellander, *Electrochim. Acta* **43**(10-11), 1447 (1998).

¹⁰ Y. T. Kim and E. S. Smotkin, *Solid State Ionics* **149**(1-2), 29 (2002).

¹¹ J. H. Shin, W. A. Henderson, and S. Passerini, *Electrochim. Commun.* **5**(12), 1016 (2003).

¹² D. Adam, *Nature* **407**(6807), 938 (2000).

¹³ D. R. MacFarlane, J. H. Huang, and M. Forsyth, *Nature* **402**(6763), 792 (1999).

¹⁴ D. Diddens, A. Heuer, and O. Borodin, *Macromolecules* **43**(4), 2028 (2010).

¹⁵ P. E. Rouse, *J. Chem. Phys.* **21**(7), 1272 (1953).

¹⁶ A. Nitzan and M. A. Ratner, *J. Phys. Chem.* **98**(7), 1765 (1994).

¹⁷ D. A. Case, T. A. Darden, T. E. Cheatham, C. L. Simmerling, J. Wang, R. E. Duke, R. Luo, M. Crowley, R. C. Walker, W. Zhang, K. M. Merz, B. Wang, *et al.*, *Amber 10* (University of California, San Francisco, 2008), URL <http://amber.scripps.edu/#Amber10>.

¹⁸ O. Borodin and G. D. Smith, *J. Phys. Chem. B* **110**(12),

- 6279 (2006).
- ¹⁹ O. Borodin and G. D. Smith, *J. Phys. Chem. B* **110**(12), 6293 (2006).
- ²⁰ O. Borodin and G. D. Smith, *J. Phys. Chem. B* **110**(23), 11481 (2006).
- ²¹ H. J. C. Berendsen, J. P. M. Postma, W. F. van Gunsteren, A. DiNola, and J. R. Haak, *J. Chem. Phys.* **81**(8), 3684 (1984).
- ²² J. P. Ryckaert, G. Ciccotti, and H. J. C. Berendsen, *J. Comput. Phys.* **23**(3), 327 (1977).
- ²³ D. van Belle, M. Froeyen, G. Lippens, and S. J. Wodak, *Mol. Phys.* **77**(2), 239 (1992).
- ²⁴ G. Mao, M.-L. Saboungi, D. L. Price, M. B. Armand, and W. S. Howells, *Physical Review Letters* **84**(24), 5536 (2000).
- ²⁵ P. Johansson, J. Tegenfeld, and J. Lindgren, *Polymer* **40**, 4399 (1999).
- ²⁶ A. G. Baboul, P. C. Redfern, A. Sutjianto, and L. A. Curtiss, *Journal of the American Chemical Society* **121**(31), 7220 (1999).
- ²⁷ A. Maitra and A. Heuer, *Macromolecular Chemistry and Physics* **208**(19-20), 2215 (2007).
- ²⁸ M. Doi and S. F. Edwards, *The Theory of Polymer Dynamics* (Oxford Science Publications, Clarendon, Oxford, 2003).
- ²⁹ P. Ahlrichs, R. Everaers, and B. Dünweg, *Phys. Rev. E* **64**(4, Part 1) (2001).
- ³⁰ J. Shi and C. A. Vincent, *Solid State Ionics* **60**, 11 (1993).
- ³¹ A. Balducci, S. S. Jeong, G. T. Kim, S. Passerini, M. Winter, M. Schmuck, G. B. Appetecchi, R. Marcilla, D. Mecerreyes, V. Barsukov, V. Khomenko, I. Cantero, *et al.*, *J. Power Sources* **196**(22), 9719 (2011).